

Anodization of aluminum in highly viscous phosphoric acid PART 1: Investigation of anodic oxide layers by scanning electron microscopy (SEM) and *in-situ* electrochemical impedance spectroscopy (*in-situ* EIS)

Lissy Berndt^{1,2}, Malte Kleemeier¹, Karsten Thiel¹, Andreas Hartwig^{1,2}, Malte Burchardt^{1,*}

¹ Fraunhofer Institute for Manufacturing Technology and Advanced Materials IFAM, Wiener Straße 12, 28359 Bremen, Germany

² University of Bremen, Chemical Department, Leobener Str., 28359 Bremen, Germany

*E-mail: malte.burchardt@ifam.fraunhofer.de

Received: 23 March 2018 / Accepted: 29 May 2018 / Published: 5 August 2018

A newly developed self-sticking tape which can be removed without residue facilitates local anodization on aluminum in cases of repair or re-work. The most prominent difference compared to conventional bath anodization is the exceptionally high viscosity of the electrolyte employed in the anodization tape. The impact of the highly viscous electrolyte on anodization is not yet known and was therefore investigated by SEM and *in-situ* electrochemical impedance spectroscopy (*in-situ* EIS). By employing cryo-SEM it could be shown that at the late stages of tape anodization (25 min at 25 V) products of the anodization process accumulate near the anodized surface and partly block it. According to XPS analysis, the blocking layer mainly consists of organic material originating from the tape adhesive, while the concentration of aluminium ions is relatively low. The high frequency part of the *in-situ* EIS was evaluated with respect to the electrical properties which commonly characterize the barrier layer of the anodic oxide, namely its resistance and capacitance. At the beginning, the values for tape anodization are in good agreement with the data for a conventional bath anodization process. However, large deviations were found for longer anodization times. These deviations could also be attributed to a partial blocking of the anodic oxide. Using a model originally proposed by Jüttner and Lorenz [12], the degree of coverage could be precisely determined from the *in-situ* EIS data. A good agreement with the coverage data from cryo-SEM was found.

Keywords: Anodization tape, porous anodic oxide, viscous electrolyte, SEM, *in-situ* electrochemical impedance spectroscopy

1. INTRODUCTION

For aluminum, anodization in acidic solutions is widely used as a pre-treatment prior to painting or bonding. Tailored anodic oxide layers for pre-treatment consist of a compact barrier layer

at the metal/oxide interface and a porous structure on top. They enhance the performance of paints and adhesives by increasing the adhesive strength and corrosion protection. Typically, the complete surface of an aluminum part or coil is anodized by immersion in an anodization bath. In cases of repair, re-work, or the partial anodization of large components, anodization in a bath cannot be applied and there is a need for local anodization techniques.

Existing methods for local anodization involve the handling of liquid electrolytes, which represents a major risk to both the user and part due to the corrosive nature of the electrolyte [1, 2]. Therefore, the electrolyte has to be collected and the aluminum part needs to be protected against an unwanted attack by the acidic electrolyte. To overcome these issues, other methods make use of thickened electrolytes or a special apparatus that collects the electrolyte [3-5]. A disadvantage of these techniques is the need for thorough cleaning, which produces large amounts of contaminated waste water. Therefore, a novel functional pressure-sensitive adhesive tape for local anodization was developed [6]. The anodization tape consists of a water-based adhesive, which includes phosphoric acid as the anodization electrolyte and an inert metal mesh as the cathode. A schematic representation of the tape and its application have been shown in a previous publication [7]. Compared to existing methods for local anodization, the anodization tape facilitates both application and cleaning. The concept is based on a pickling tape for the surface treatment of aluminum, which has been examined previously [8].

In comparison to conventional anodization baths, the viscosity of the adhesive of the anodization tape is higher by more than six orders of magnitude. Therefore, mass transport processes associated with heterogeneous reactions at the aluminum surface (anode) and the metal mesh (cathode) are altered. This leads to reduced rates of oxide formation and dissolution compared to low viscosity electrolytes typically used in anodization baths [7]. In addition, the anodic oxide layer may be affected by the polymer components. Previous research has investigated the thicknesses of the porous oxide layer and the barrier layer as well as the morphology of the porous oxide layer formed during anodization [7].

A method which can be employed to obtain further information about the formation of an anodic oxide layer during anodization in a highly viscous electrolyte is cryo-scanning electron microscopy (cryo-SEM). Because this method operates on rapidly frozen samples, it allows a detailed investigation of the anodic oxide surface at well-defined points during the anodization process.

In addition, *in-situ* electrochemical impedance spectroscopy (*in-situ* EIS) is also used for investigation during the anodization process. EIS has also found broad application for the characterization of charge transfer and mass transport processes at electrodes. Important areas of application are electrochemical energy storage [9], organic and inorganic coatings for corrosion protection [10-12], and complex electrochemical reactions [13]. For EIS, electrochemical systems can only be investigated if they are stationary during the measurement [14]. For *in-situ* EIS during anodization with high DC offset voltages, this condition is only fulfilled if all processes are quasi stationary or if the changes are small within the timescale of the experiment. *In-situ* EIS has already been used for the investigation of anodization processes. Mazzarolo et al. examined the morphological evolution of anodic titanium oxide in 1 M sulfuric acid by means of *in-situ* EIS [15]. Curioni et al. [16] and Hua et al. [17] used aluminum as the anode and sulfuric acid as the electrolyte. Curioni et al.

focused on the ionic migration through the barrier oxide layer and Hua et al. investigated the influence of the addition of adipic acid on sulfuric acid anodization. Both conventional EIS and *in-situ* EIS provide information on the barrier oxide layer (capacitance, resistance), but the porous oxide layer has a minor influence on the impedance spectrum [16, 18].

In this paper, we present a study of anodic oxide layer formation in the highly viscous electrolyte of the anodization tape in comparison with liquid phosphoric acid-based electrolytes. For the sake of clarity, the anodization of aluminum is carried out in a conventional bath process known as “bath anodization” in the subsequent text, while the term “tape anodization” refers to the surface treatment of aluminum employing the newly developed anodization tape. Our aim was to investigate the effects of the high viscosity on the thickness and morphology of the anodic oxide. Another aspect that deserves attention is that of the ion transport processes in the electrolyte. Due to the high viscosity, reaction products (especially aluminum ions) may accumulate near the interface to the substrate, leading to a pronounced “local aging” of the electrolyte. In order to obtain a detailed picture of the processes involved, we combined *in-situ* EIS as an electrochemical analysis technique with imaging methods like transmission electron microscopy (TEM), cryo-SEM, and energy dispersive X-ray spectroscopy (EDX). Each individual technique has already been proven to be useful for analyzing the anodization of aluminum; however, in this work, for the first time, they are used jointly in order to elucidate the effects that occur under the condition of very high viscosity.

2. EXPERIMENTAL

2.1 Samples and electrolytes

For tape anodization, sheets of commercially pure aluminum (AA1050A) were used as substrates because of its technical importance and the low concentration of chemical impurities which could influence the anodization process. The nominal composition is given in Table 1 (EN 573-3).

Table 1 Nominal composition of aluminum AA1050A

Chemical element	Al / wt.%	Fe / wt.%	Si / wt.%	Zn / wt.%	Cu / wt.%	Mn / wt.%	Mg / wt.%	Ti / wt.%
AA1050	99.5	0.26	0.08	0.002	0.002	0.005	0.004	0.021

Through a multi-stage cleaning process (Table 2), clean and reproducible surfaces were obtained prior to anodization. In between all steps, the samples were spray rinsed with deionized (DI) water (30 s – 45 s).

Table 2 Multi-stage cleaning of specimens for tape anodization

Stage of cleaning	Solution composition	Temperature / °C	Time / min
Degreasing	40 g L ⁻¹ Turco 4215 NC (Henkel) in water	60	5
Rinsing	Deionized (DI) water	room temperature (RT)	3
Etching	40 g L ⁻¹ Aluminetch No. 2 (Henkel) in water	60	1
Rinsing	DI water	RT	3
Pickling	180 mL L ⁻¹ Turco Liquid Smutgo NC (Henkel) in water	36	10
Rinsing	DI water	RT	3
Drying	-	50	30

After cleaning, the specimens were stored in an argon atmosphere until the application of the anodization tape.

The substrates for bath anodization in phosphoric acid (phosphoric acid anodization, PAA) were also made of aluminum AA1050A (Table 1). A disc of AA1050A about 1 cm in diameter was inserted in a polytetrafluoroethylene or polyetheretherketone holder (2 cm diameter). The embedded aluminum discs were grinded with silicon carbide abrasive paper (2500 and 4000 grit). Subsequently, the aluminum surfaces were polished with a rugged synthetic fabric MD-Plus (Struers) and a diamond-based suspension with a particle size of 3 µm. A mixture of ethanol and ethylene glycol was used as a cooling medium. For finishing, the electrode surfaces were polished with neoprene fabric MD-Chem (Struers) and a polishing agent, namely silica suspension with a particle size of 0.04 µm. Subsequently, the specimens were rinsed in DI water and small amounts of polishing agent were removed using ethanol. In order to obtain a reproducible natural oxide layer, specimens were kept in a desiccator with a drying agent (silica gel) for at least 24 h after mechanical treatment. Immediately prior to bath anodization, specimens were pickled in 180 mL L⁻¹ Turco Liquid Smutgo NC (Henkel) for 10 min at 36 °C and rinsed in DI water for 3 min at RT to obtain an initial state comparable to that of the substrates for tape anodization.

The concentration of phosphoric acid for PAA was 12 wt.%.

The adhesive for the anodization tape was prepared from polyvinyl alcohol (Mowiol 10-98, Kuraray), polyacrylic acid 40 wt.% solution in water (DEGAPAS 4104S, Evonik), fumed silica (Aerosil 200, Evonik), lactic acid, glycerol, and phosphoric acid 85% (the latter three chemicals were obtained from Sigma-Aldrich). More details on the preparation of anodization tapes can be found in a previous publication [7].

2.2 Determination of the viscosity of the electrolytes used for the anodization bath and anodization tape

Rheological measurements were carried out at 25 °C using a Bohlin Gemini 200 rheometer (Malvern Instruments, UK). For the liquid samples (bath anodization), a coaxial cylinder geometry

with a gap size of 150 μm was chosen. In the range of 1 – 50 1/s shear rates, the samples behaved as Newtonian liquids, i.e. the measured viscosity was independent of the applied shear rate. Therefore, the reported viscosity values are averages over all data collected in this range of shear rates. For the highly viscous adhesive of the anodizing tape, viscosities were determined in plate-plate geometry (plate diameter 8 mm). A sample was cut from the anodizing tape and fixed to the lower plate. The upper plate was pressed onto the adhesive layer of the tape with a normal force of 200 mN, resulting in a gap of about 900 μm . Measurements were conducted in oscillatory mode with a frequency of 1 Hz and a deformation of 0.01. The reported value is an average of two measurements on individual specimens of the anodizing tape.

Table 3 Electrolyte viscosity of the anodization bath and the anodization tape (mPa s)

	Bath anodization	Tape anodization
Electrolyte viscosity / mPa s	1.2	10^7

2.3 Anodization and *in-situ* EIS

For all anodization processes and *in-situ* EIS, a potentiostat GAMRY Reference 3000 was used in the high voltage regime, controlled by a personal computer using the GAMRY Framework software package 6.20. Bath anodization was performed in a top mounted cell with a volume of 20 ml on the embedded aluminum discs in order to avoid the accumulation of gas bubbles on the working electrode. A three-electrode-cell setup was used with a platinum sheet as counter electrode and a saturated calomel electrode (SCE) as reference electrode in a non-stirred solution. At the beginning of the anodization, the temperature of the electrolyte was 20 °C and, due to the reaction, the electrolyte was heated to 23 °C. Fresh electrolyte was used for each bath anodization.

For tape anodization, the tape was applied to an aluminum specimen and the steel mesh (cathode) in the anodization tape and the aluminum part were connected to the potentiostat in a two-electrode setup. All potentials listed in this paper are referred to as SCE. For readability, the term “voltage” is used synonymously for potentials in a three-electrode setup and voltages in a two-electrode setup. The conditions in the laboratory were in the range of 21 ± 2 °C and $50 \pm 10\%$ RH.

After bath and tape anodization, the samples were carefully rinsed in DI water and immersed in DI water in an ultrasonic bath for 5 min.

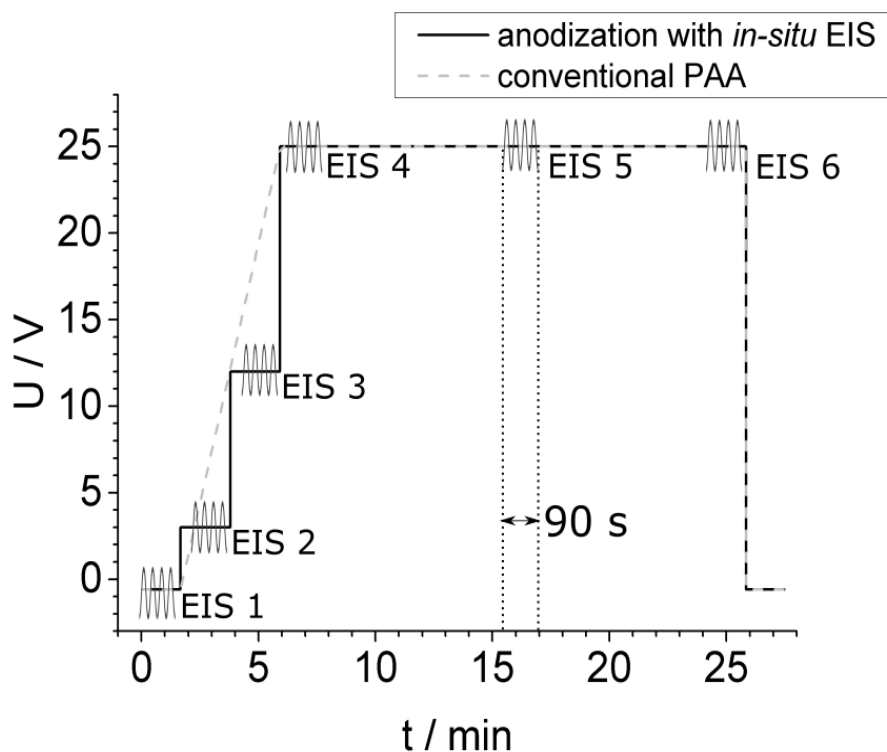


Figure 1. Schematic representation of the anodization process with *in-situ* EIS

In-situ EIS measurements during bath anodization and tape anodization were carried out with the same setup of the electrochemical cells. The sequence of the electrochemical steps is schematically depicted in Figure 1 and corresponds to a conventional PAA process with a 6 V min^{-1} voltage ramp from open circuit potential (OCP) to 25 V and a 20 min voltage plateau. The voltage ramp was approximated by 3 voltage steps from OCP to 3 V, to 12 V, and to 25 V. The duration of the steps was about 125 s. Deviations of step times were caused by different periods of the EIS measurements in the slow frequency range. One EIS measurement at every voltage step was carried out after an equilibration time of 30 s (EIS 2 – EIS 4). Additional EIS measurements were carried out at 25 V and started after 15.5 min (EIS 5) and 24.6 min (EIS 6). EIS was also recorded at OCP prior to anodization (EIS 1). All measurements were carried out in the anodization electrolytes. The frequency range for EIS was 100 kHz to 0.16 Hz with 5 measurements per decade, which required approximately 90 s. AC peak-to-peak voltage was 20 mV (7.07 mV rms).

Experimental impedance spectra were fitted to equivalent electrical circuits using the GAMRY Echem Analyst software and a simplex fit routine.

2.4 Focused ion beam (FIB)

For the nanostructural analysis of the barrier layer of the anodic oxide using the transmission electron microscope (TEM), thin electron transparent lamellas first needed to be prepared. Samples were taken from the anodization process at the half time of each EIS measurement (EIS 2 to EIS 6). This was achieved by focusing the ion beam preparation with a Ga ion beam in a FEI Helios 600 dualbeam machine. The procedure was as follows: first a few nanometers of Pt/Pd were deposited on

the surface to prevent charging of the sample in the FIB in a Cressington Turbo sputter coater 208 (Watford, UK). After introducing the sample into the FIB, 500 nm carbon was deposited onto the surface by means of electron beam induced deposition (in one case platinum was used; see Figure 3), followed by an additional 3-4 μm of carbon deposited by means of ion beam induced deposition. This approach ensures that the uppermost features of the oxide are preserved during the FIB preparation. Then the standard procedure of TEM lamella preparation by FIB was carried out by cutting a relatively thick lamella (at 30 kV ion beam energy), transferring and mounting it to an Omniprobe TEM grid, further thinning it to electron transparency, and finally polishing the lamella (at 5 kV ion beam energy). TEM lamellas prepared this way usually have a final thickness of below 50 nm.

Due to the fact that the porous oxide layer leads to pronounced curtaining of the lamella in the preparation process, the lamella was rotated 180 degrees in the FIB so that the inevitable curtains ran from the oxide into the protection layer and not across the barrier layer into the substrate.

2.5 Transmission electron microscopy (TEM)

To analyze the structure and size of the barrier layer of the oxide, TEM was carried out using a FEI Tecnai F20 S-TWIN microscope (Hillsboro, USA) equipped with a field-emission gun (FEG). The microscope was operated at an accelerating voltage of 200 kV, resulting in a point resolution of 2.4 Å. The TEM images were recorded with the slow-scan CCD camera integrated in a Gatan image filter (GIF2001, 1024x1024 pixel array). Elemental analysis was carried out by operating the TEM in scanning mode (STEM) with a spatial resolution of 1-2nm. STEM images were recorded with a high-angle annular dark field (HAADF) STEM detector. EDX spectra analysis was executed out using an EDAX r-TEM-EDX-Detector with an energy resolution of 136eV, measured at Mn-K α .

2.6 Cryo-scanning electron microscopy (Cryo-SEM)

Cryo-SEM work was carried out using the Quorum PP2000T cryo-SEM preparation system (Laughton, UK) attached to a FEI Helios 600 dualbeam machine (Hillsboro, USA). After anodizing, the samples were initially shock frozen and kept in liquid nitrogen. These pre-frozen specimens were then loaded onto on specimen stub, again in liquid nitrogen, and carried under a vacuum condition into the cryo-preparation chamber. Here, the sample holder was kept at -130 °C while the rest of the chamber had a temperature of -196 °C. This setup inhibits contamination build-up on the sample surface. To remove ice on the sample surface, the sample was heated to -90 °C for 5 min. After that, a thin film of platinum was sputtered on the sample surface in the preparation chamber to prevent charging of the sample surface in the SEM. Finally, the sample was transferred into the SEM, where the sample temperature was again held at -130 °C while a cryo-shield in the SEM chamber near the pole piece was held at -160 to -170 °C to prevent contamination of the sample surface. Details of the acquisition parameters of the images can be found in the info banner under the respective SEM image. EDX spectra were recorded using an Oxford X-max 80 SD-detector (Abingdon, UK) with a resolution of 125 eV measured at Mn-K α .

3. RESULTS AND DISCUSSION

Anodization was carried out in baths and with the anodization tape. The current density-time responses in the bath and with the anodization tape during anodization with *in-situ* EIS are shown in Figure 2.

Current density is a measure of oxide formation during anodization. It comprises oxide formation (increasing barrier layer thickness with increasing voltage) and oxide re-formation due to dissolution. At a constant voltage and under stationary conditions, current density is equal to the dissolution current, which is – in the first approximation – responsible for the growth of the porous part of the anodic oxide. Right after each voltage step, the current density abruptly increased due to the charging of the electrochemical double layer and the thickening of the barrier oxide layer. Subsequently, current density decreased quickly due to the continuous thickening of the barrier layer [19]. After passing a local minimum of the current density, which is associated to pore nucleation and formation of the classical porous oxide morphology [19], an almost constant current density was reached after approx. 60 s. The variations of current density were below 15 %.

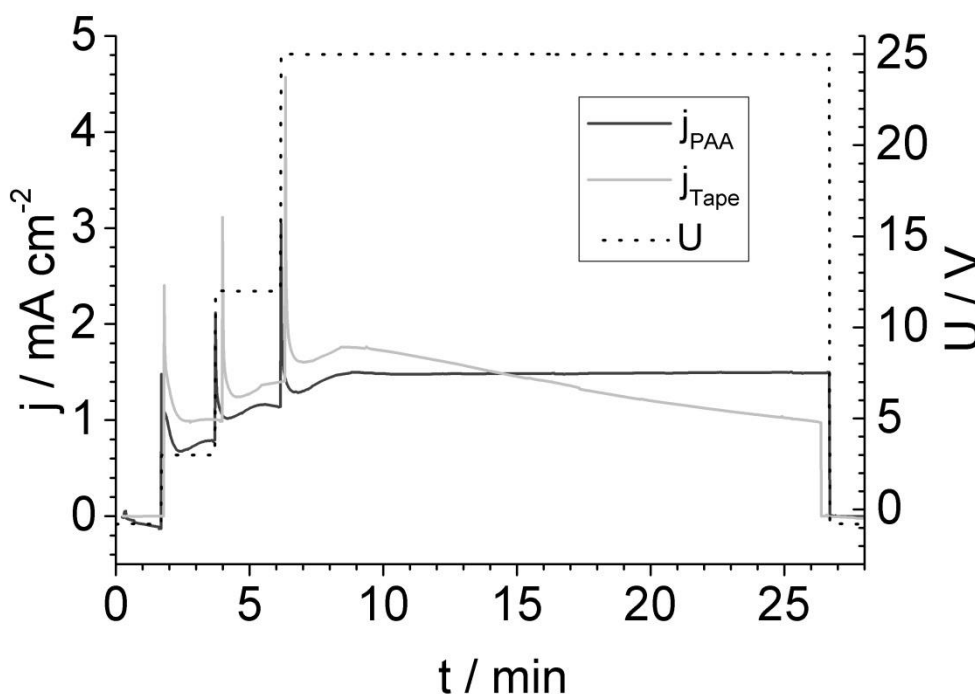


Figure 2. Voltage curve and current density-time response for the anodization of AA1050 at 20 °C, 25 V, 6 V min⁻¹, 20 min for bath (dark grey) and tape anodization (light grey)

In comparison to conventional bath anodization, current densities for tape anodization are slightly higher during the stepwise increase of the voltage. During the voltage plateau (25 V), current density is almost constant for bath anodization, whereas it decreases constantly for the anodization tape. Macroscopic detachment of the anodization tape from the aluminum substrate (e.g. due to oxygen formation at the anode) was not observed during the experiments. Therefore, it is more likely that this

observation can be associated with the partial blocking of the active sites of the anodic oxide (*vide infra*).

The morphology of porous oxide layers on aluminum AA1050A was evaluated by transmission electron microscopy (TEM). As an example, the anodic oxide layers obtained at the beginning of the plateau voltage (25 V) are shown in Figure 3.

In addition to the porous part of the anodic oxide, the barrier layer at the metal/oxide interface can be clearly seen. Despite the preparation by FIB, leading to a thickness as less as 50 nm, the TEM lamellae are so thick that several pores in a series are represented. The porous oxide layer at EIS 4 consists of 3 parts with different pore diameters. These layers are formed due to the abrupt change in voltage in the step-like voltage evolution from 3 V to 12 V and to 25 V, because the pore diameter is linearly dependent on the applied voltage [7, 20]

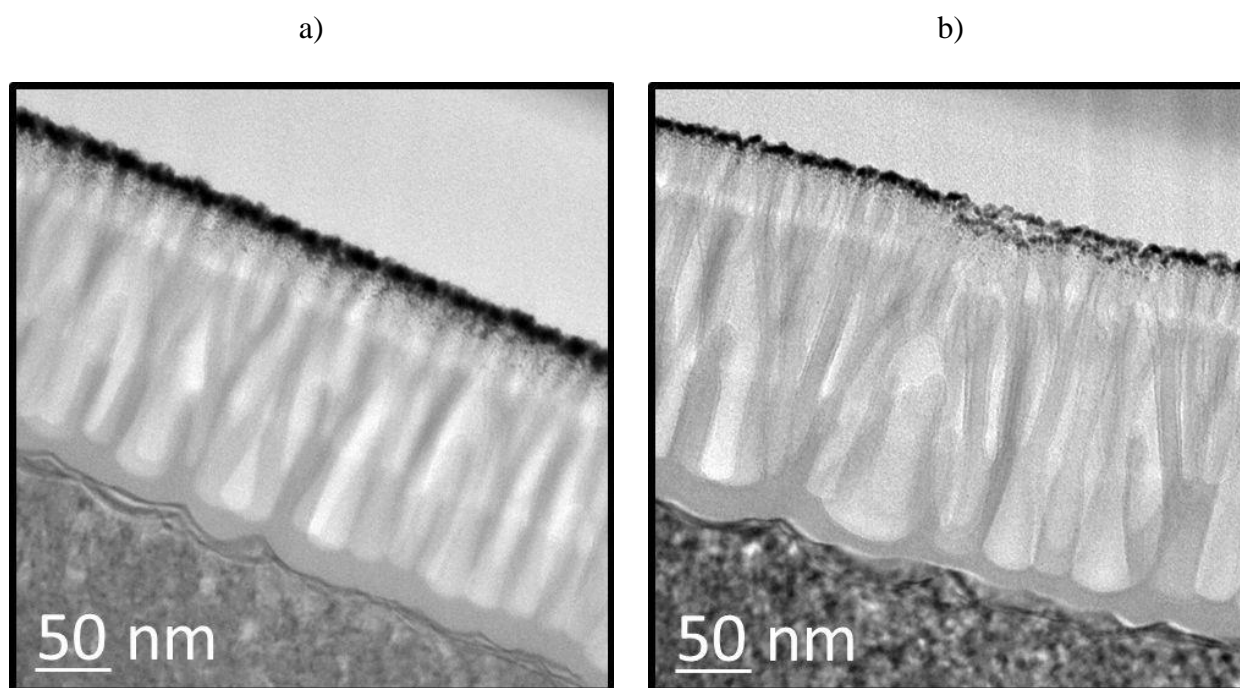


Figure 3. TEM micrographs of anodic oxide layers from test specimens taken at EIS 4 (25 V); a) bath anodization; b) anodization tape; bottom: metal; center: anodic oxide layer; the dark area on top of the oxide layer consists of platinum that is applied to ensure neutralization of the sample surface during SEM investigation and FIB preparation

At the end of the anodization (EIS 6), the total layer thickness of the anodic oxide is 1250 nm for bath anodization and 950 nm for tape anodization. The thicknesses of the individual layers of the porous part of the anodic oxide are identical for the sublayers at 3 V and 12 V. The thicknesses of the barrier type oxide layers (32 nm) are also identical for bath and tape anodization. Differences between bath and tape anodization can be found for longer treatment times at 25 V. The sublayer for 20 min at 25 V for tape anodization with 810 nm is clearly thinner than the same sublayer for bath anodization with 1130 nm. This observation is in agreement with the decrease in the current density of tape anodization during the voltage hold at 25 V, but a distinct explanation for the decrease cannot be

deduced. The measurements were repeated at different positions of the samples and showed similar results.

The investigation by TEM also allows the estimation of the barrier layer thickness of the obtained oxide layers (Figure 4).

As a result of the increasing voltage, the barrier layer thickness increases from EIS 2 (3 V) to EIS 4 (25 V) from 6.4 nm to 31.1 nm. For the constant voltage of 25 V (EIS 4 – EIS 6), no further changes of barrier layer thickness were observed (Table 5).

To obtain further information about the decrease of current density and mass transport for tape anodization, the non-standard method of cryo-SEM was applied. Specimens were anodized by tape anodization until EIS 4, EIS 5 and EIS 6 (Figure 1). After anodization, the tape was removed and the specimens were frozen in liquid nitrogen without prior rinsing in DI water. Freezing preserves the condition of the sample surface directly after anodization and leads to a snapshot of the process. The frozen samples were examined with SEM and the oxide surfaces were investigated (Figure 5).

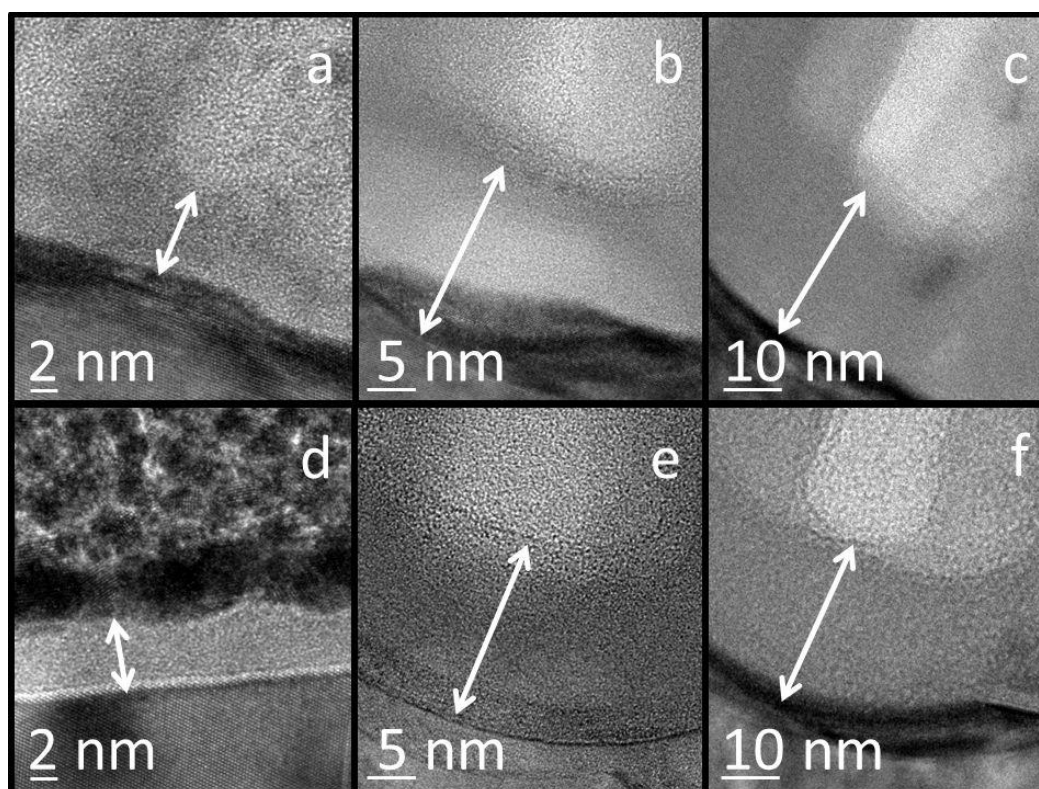


Figure 4. TEM images of the barrier layer (white arrow) of the anodic oxide obtained in bath (a-c) and tape anodization (d-f) at EIS 2, 3 V (a+d), at EIS 3, 12 V (b+e), and at EIS 4, 25V (c+f)

In Figure 5a, most of the surface under investigation has the typical appearance of a porous anodic oxide. As can be deduced from the high magnification images (Figure 5d), the island-like dark areas correspond to porous anodic oxide that is plugged by residues of the anodization tape. The open anodic oxide (bright areas) of EIS 4 (25 V, 30s) in Figure 5a corresponds to 80% of the area under investigation.

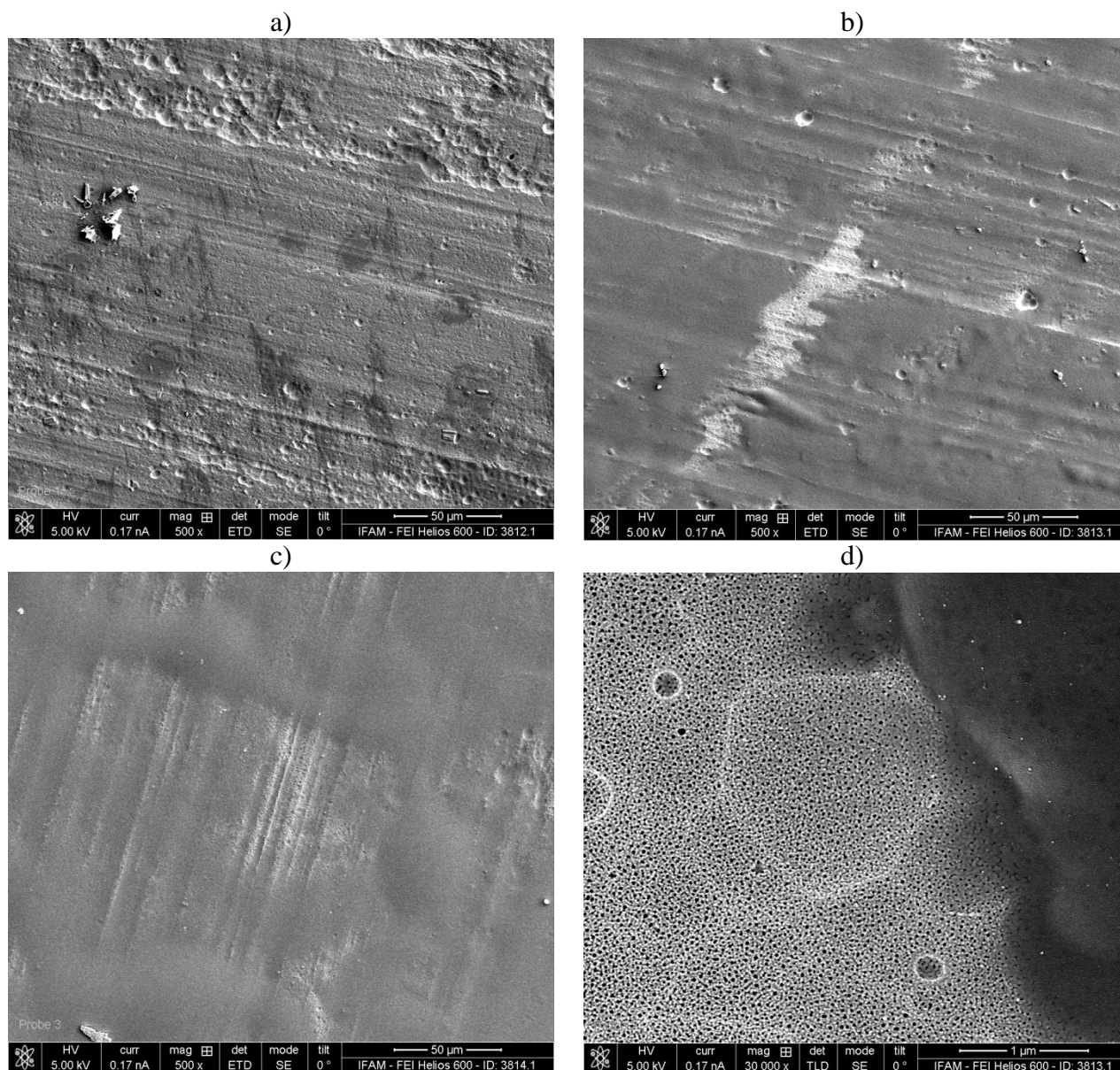


Figure 5. SEM plan view micrographs of the anodic oxide layers from test specimens taken at a) EIS 4 (25 V, 30 s), b) EIS 5 (25 V, 10 min), and c) EIS 6 (25 V, 20 min) prepared by tape anodization; d) EIS 5 (25 V, 10 min) as a high magnification image; light areas correspond to anodic oxide and dark areas correspond to polymeric components on the anodic oxide

The appearance of the sample surface after 10 and 20 min anodization time (Figure 5b and Figure 5c) is completely different. The surface is covered by a cloud-like layer and only about 40% for EIS 5 (25 V, 10 min) and 20% for EIS 6 (25 V, 20 min) of the underlying anodic oxide is visible. The cloud-like layer seems to have a considerable thickness, because the underlying rolling marks of the aluminum substrate are completely hidden.

As indicated by EDX analysis, the cloud-like layer for EIS 6 consists mostly of organic compounds and has a high phosphorous content (Table 4).

Table 4. Chemical composition of the aluminum surface after tape anodization without cleaning at EIS 4 (25 V, 30s) and EIS 6 (25 V, 20 min); data obtained by EDX measurement with 10 kV (area of investigation: 518 μm x 453 μm)

	O / at. %	Al / at. %	C / at. %	P / at. %
EIS 4	51.4	33.1	11.4	3.7
EIS 6	68.8	7.0	15.7	8.4

It can be assumed that the cloud-like layer is formed by the residues of the aged tape electrolyte. EDX analysis does not indicate an especially high amount of aluminum in the cloud-like layer, as the concentration of aluminum is reduced by 80% compared to EIS 4 (Table 4). It cannot be excluded yet that the properties of the covering layer are strongly modified even by a low amount of aluminum ions. As an example, the literature discusses the chemical crosslinking of polyacrylic acid and polyvinyl alcohol by aluminum ions [25-27].

The formation of a cloud-like layer on top of the porous oxide during tape anodization can effectively reduce the active area of current flow and therefore allows an explanation for the decreasing current density during tape anodization. It should be noted, however, that the cloud-like layer probably has no static structure but rather seems to fluctuate with time. If the cloud-like layer were static, it could be expected that the thickness of the oxide layer below the residues would be significantly lower than in areas not covered by residues. In effect, residues with static structure should leave an imprint on the anodic oxide layer. However, this was not observed. Careful examination of the oxide layer revealed that the thickness of the anodic oxide layer is uniform over the whole sample surface.

Further investigations are certainly needed to elucidate more details of the cloud-like layer. Investigations by SEM deliver only “snapshots” of the cloud-like layer, and the degree of coverage cannot be determined with high accuracy due to the fuzzy shape of the residues. Additionally, specimen preparation for cryo-SEM is complex and therefore not well suited to continuously monitoring the degree of coverage.

In the following it will be shown that *in-situ* EIS is a complementary method to cryo-SEM and offers an elegant way to determine the degree of coverage during the tape anodization process.

During bath anodization and tape anodization, five EIS spectra – EIS 2 to EIS 6 – were recorded during the voltage ramp (approximated by a step-like voltage evolution) and the plateau voltage (Figure 1). Furthermore, EIS were recorded prior to anodization (EIS 1). Figure 6 shows the Nyquist plots of EIS spectra EIS 1 to EIS 6 for bath and tape anodization.

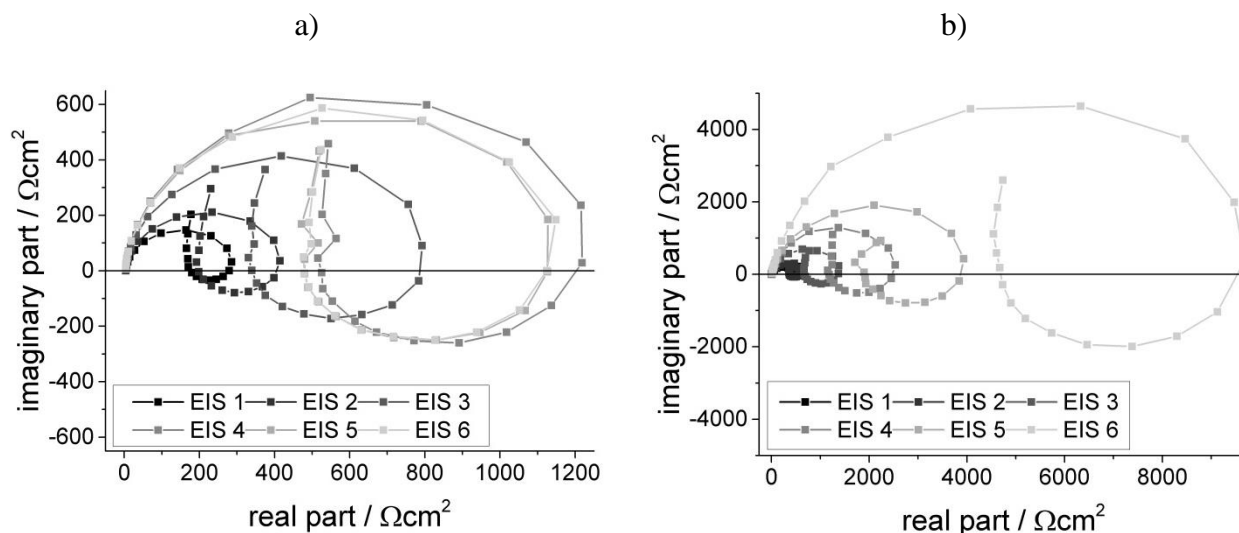


Figure 6. Nyquist plots of *in-situ* EIS during anodization at EIS 1 (OCP), EIS 2 (3 V), EIS 3 (12 V), EIS 4 (25 V, 30 s), EIS 5 (25 V, 10 min) and EIS 6 (25V, 20 min); a) bath anodization; b) tape anodization; symbols represent experimental values; lines serve as a visual guideline

The shape of the Nyquist plots is similar for bath and tape anodization. Three loops are visible: The high frequency part ($10^5 - 10^3$ Hz, capacitance), the medium frequency part ($10^2 - 1^0$ Hz, inductivity with $\varphi > 0^\circ$, and $Z_{lm} < 0$ Ohm), and the low frequency part (< 1 Hz, capacitance). This shape with two or three loops, which depends on the measured frequency range, were also found by other research groups in corrosive media [28-35] or for *in-situ* EIS with a distinct current flow [16, 17].

The quality of the EIS data is good: Throughout all measurements, low noise/fluctuation were observed. This might be due to the low overall resistance of the system and the limited frequency range (lowest frequency 0.16 Hz), but it also indicates that samples were quasi-stationary (variation in current density was below 15 %) during the time frame of the experiment. This quasi stationarity is fundamental for *in-situ* EIS measurements.

For increasing the voltage/treatment time, the diameter of the high frequency capacitive loop in the Nyquist plot (or $|Z|_{3000\text{ Hz}}$ in the Bode plot) increases, which is associated with an increasing resistance of the barrier oxide layer. In contrast, it has been reported that for *in-situ* EIS during anodization or the variation of potential in sulfuric acid, the high frequency loop in the Nyquist plot becomes smaller with increasing potential [16, 17]. We were able to reproduce the results in sulfuric acid, thereby excluding that other experimental settings that led to the different behavior. A possible reason could be the different dielectric properties and growth kinetics of the barrier layer of the anodic oxides formed in sulfuric and phosphoric acid. Another reason could be a higher dissolution current in sulfuric acid, which leads to a smaller resistance of the barrier layer.

From the Nyquist plot (Figure 6a and Figure 6b) it can be deduced that the impedance of tape anodization is significantly higher than the impedance of bath anodization. While bath anodization reveals similar EIS spectra for constant voltage (25 V, EIS 4 – EIS 6), impedance is strongly increasing for tape anodization.

Similar to the EIS measurement under stationary conditions, the capacitive loop in the high frequency range is consistently associated with the properties of the barrier layer oxide in the literature [32, 33, 35]. The inductive loop and the second capacitive loop are related to different phenomena and are controversially discussed. Some authors relate the system's response to electrochemical reactions between the different ionic species to the processes of oxide dissolution, oxide formation and nucleation [28, 33, 36-38]. Others correlate the low frequency loops to mass transport processes involving adsorption and relaxation processes [31, 34, 35, 39-41]. In this work we restrict our data analysis to the high frequency range (10^5 to 100 Hz). It will turn out that this is appropriate to extract the important properties of the oxide as well the coverage of the oxide layer by residues from the anodization medium. An attempt to analyze the full frequency range is complicated by the fact that there is currently no equivalent circuit model that is commonly accepted in the literature. Different models with moderate to high complexity exist. However, to the best of our knowledge, no such model takes into account a partial blocking of the anodic oxide surface by residues.

We begin our data analysis by applying a strongly simplified equivalent electrical circuit for fitting the *in-situ* EIS spectra (Figure 7). It consists of the electrolyte resistance ($R_{\text{electrolyte}}$), the porous part of the anodic oxide (R_{pores}), and the barrier oxide (R_{barrier} , C_{barrier}). This assignment is similar to the models for EIS of aluminum oxide under stationary conditions in the literature [42]. The capacitance is often replaced by a constant phase element (CPE), reflecting the non-ideal behavior of typical samples and experimental setups [12, 43].

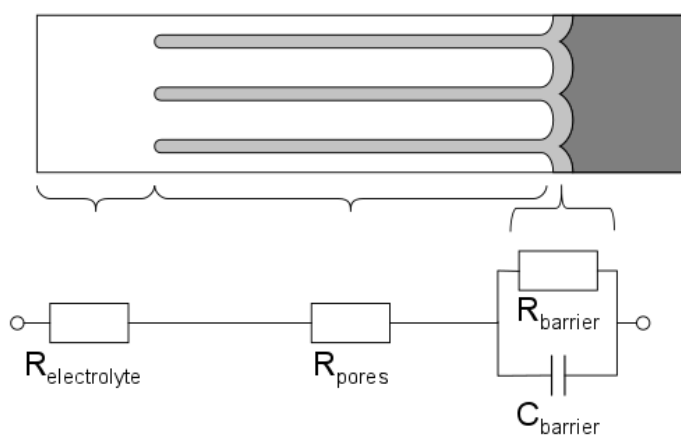


Figure 7. Simplified equivalent electrical circuit for fitting data from *in-situ* EIS during anodization of aluminum in phosphoric acid containing electrolytes (not to scale)

The electrolyte resistance is given as the distance between anode and cathode $d_{\text{electrolyte}}$, the electrolyte conductivity κ , and the area of the working electrode A ,

$$R_{\text{electrolyte}} = \frac{d_{\text{electrolyte}}}{A \cdot \kappa} \tag{1}$$

whereas pore resistance R_{pores} is determined by the oxide layer thickness d_{barrier} and the porosity of the anodic oxide ϕ (Eq. 2),

$$R_{\text{pores}} = \frac{d_{\text{pores}}}{\phi \cdot A \cdot \kappa} \tag{2}$$

with

$$\Phi = \frac{A_{\text{pores}}}{A_{\text{complete}}} \tag{3}$$

where A_{pores} is the area of the pore opening and A_{complete} is the total area under investigation (pore opening and pore walls).

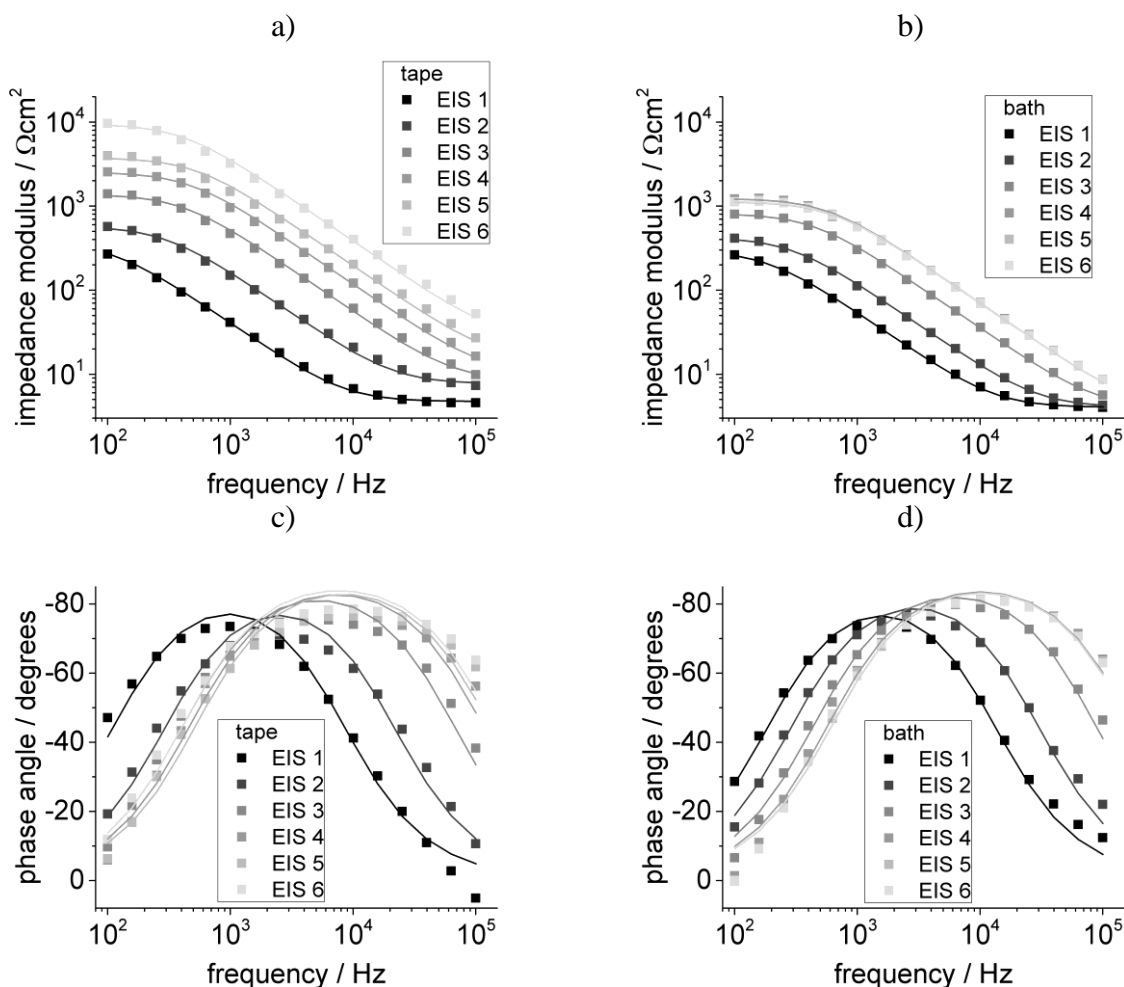


Figure 8. Bode plots of impedance modulus of in-situ EIS during a) tape and b) bath anodization at EIS 1 (OCP), EIS 2 (3 V), EIS 3 (12 V), EIS 4 (25 V, 30 s), EIS 5 (25 V, 10 min), EIS 6 (25 V, 20 min); corresponding Bode plots of phase angle of c) tape and d) bath anodization; symbols represent experimental values; solid lines were fit results obtained by fitting the experimental data with the equivalent circuit from Figure 7

In order to estimate pore resistance R_{pore} in relation to the electrolyte resistance $R_{\text{electrolyte}}$, porosity Φ was evaluated according to Eq. (3) from the SEM top view images. Due to sputtering and the enhancement of edges in SEM images, the proportion of pore walls might have been overestimated, and for simplification it was assumed that the pore opening at the surface describes the diameter of the pore at the pore bottom.

The anodic oxide produced by bath and tape anodization had a relatively open structure. For example, bath anodization at 25 V, with 6 V min^{-1} ramp and 20 min hold, resulted in an oxide layer with a porosity of about 54%. Taking into account that the maximum oxide layer thickness is in the

range of 1000 nm while the distance between cathode and anode is at least 1 mm, it can be concluded that $R_{\text{electrolyte}}/R_{\text{pores}} > 500$. Therefore, the pore resistance is negligible in comparison with the electrolyte resistance and is insignificant for the fit.

The barrier layer can be interpreted as a parallel plate capacitor with the barrier layer as dielectric medium with the thickness d_{barrier} . The capacitance C_{barrier} , normalized to the electrode area A , can be represented by Eq. (4).

$$C_{\text{barrier}} = \frac{C'}{A} = \frac{\epsilon_0 \cdot \epsilon_r}{d_{\text{barrier}}} \tag{4}$$

ϵ_0 and ϵ_r represent the permittivity of the vacuum ($\epsilon_0 = 8.854 \cdot 10^{-14} \text{ F cm}^{-1}$) and the relative dielectric number of aluminum oxide.

The experimental data were fitted to the equivalent electrical circuit presented in Figure 7. In general, agreeable fits for EIS 1 to EIS 6 were obtained. Plots of the experimental data and fit results for bath and tape anodization are shown in Figure 8.

The fitting results for barrier layer capacitance C_{barrier} and barrier layer resistance R_{barrier} are presented in Table 5a for bath anodization and in Table 5b for tape anodization for EIS 2 to EIS 6.

Table 5. Layer capacitance, layer resistance, dielectric constant and layer thickness of barrier oxide formed by a) bath and b) tape anodization

a) Bath anodization		EIS 2 (3 V)	EIS 3 (12 V)	EIS 4 (25 V)	EIS 5 (25 V)	EIS 6 (25 V)
TEM	Barrier layer thickness $d_{\text{barrier}} / \text{nm}$	6.4	20.6	31.1	32.3	31.9
EIS	Barrier layer capacitance $C_{\text{barrier}} / 10^{-7} \text{ F cm}^{-2}$	13.02 ± 0.14	4.45 ± 0.07	2.24 ± 0.04	2.26 ± 0.04	2.26 ± 0.03
	Barrier layer resistance $R_{\text{barrier}} / \Omega \text{ cm}^2$	420 ± 5	800 ± 1	1230 ± 10	1120 ± 5	1130 ± 10
	Relative dielectric number ϵ	9.4	10.3	7.9	8.2	8.1

b) Tape anodization		EIS 2 (3 V)	EIS 3 (12 V)	EIS 4 (25 V)	EIS 5 (25 V)	EIS 6 (25 V)
TEM	Barrier layer thickness $d_{\text{barrier}} / \text{nm}$	4.6	19.2	33.2	32.9	31.3
EIS	Barrier layer capacitance $C_{\text{barrier}} / 10^{-7} \text{ F cm}^{-2}$	10.06 ± 1.60	3.22 ± 0.50	0.15 ± 0.27	0.09 ± 0.13	0.06 ± 0.21
	Barrier layer resistance $R_{\text{barrier}} / \Omega \text{ cm}^2$	490 ± 100	1180 ± 250	2160 ± 490	3270 ± 640	7070 ± 3200

As a consequence of the growth of the barrier layer, the barrier resistance R_{barrier} increases and the barrier capacitance C_{barrier} decreases with increasing voltage from EIS 2 to EIS 4. At a constant

voltage (EIS 4 to EIS 6), barrier layer resistance and barrier layer capacitance are constant Table 5a. These observations are valid for bath anodization. For tape anodization, oxide resistance increases and oxide capacitance decreases with increasing and constant voltage.

Barrier layer resistance at EIS 6 for bath anodization ($1.13 \times 10^3 \Omega \text{ cm}^2$) is very low for a barrier layer thickness of 31 nm (see in Table 5a). A typical value of $0.22 \times 10^6 \Omega \text{ cm}^2$ for barrier resistance on AA1050 with a barrier layer thickness of 26 nm, which was formed in 0.8 mol phosphoric acid and at a voltage of 15 V, is published by Dasquet et al. [44]. The low resistance of barrier layer for EIS 6 can be explained by the existence of mobile ions under the high field applied during *in-situ* EIS. Curioni et al. have investigated the dependence of barrier resistance on the applied voltage. For 16 V in sulfuric acid they obtained a barrier resistance of about $500 \Omega \text{ cm}^2$ [16].

Using the capacitance evaluated from the EIS and the barrier layer thickness obtained from the TEM images (Figure 4), the relative dielectric number ϵ_r of the aluminum oxide can be calculated. The relative dielectric number ϵ_r was calculated according to Eq. (4) using the geometric area of the flat panel electrochemical cell. The relative dielectric numbers calculated from the barrier layer thickness of TEM and the oxide capacitance of EIS are shown in Table 5a.

During the voltage ramp, the relative dielectric numbers (9.4 at EIS 2 and 10.3 at EIS 3) are slightly higher than during the voltage hold (7.9 to 8.2). In the literature, relative dielectric numbers of aluminum oxide formed by anodization are reported to be in the range of 7.5 to 15 [45].

From EIS 2 ($U = 3 \text{ V}$) to EIS 4 ($U = 25 \text{ V}$), the thickness of the barrier layer increases for bath and tape anodization (Table 5a and b). This is in agreement with the linear dependence of the barrier oxide layer thickness on the voltage [7, 23, 24]. The formation factor k

$$k = \frac{d}{(U - U_0)} \quad (5)$$

is around 1.2 nm/V, with U_0 being the (extrapolated) voltage for $d = 0$. The barrier layer thicknesses of EIS 5 and EIS 6 (constant voltage) are identical to that of EIS 4 (Table 5). The formation factor is identical for bath and tape anodization.

A different evolution of oxide morphology for bath anodization and tape anodization can be identified from the TEM images of EIS 2 samples. While for tape anodization only a barrier layer with a waved surface (Figure 4d) is observed, for bath anodization a porous structure is formed. For EIS 3 and subsequent samples, a porous structure is also found for tape anodization. The different onset of pore formation can be explained by the faster mass transport of ionic species for bath anodization due to the lower electrolyte viscosity and lower electrical resistance.

For tape anodization, special trends are detected for the resistance and capacitance of the barrier layer at the plateau voltage. The increasing resistance at the plateau voltage from $1000 \Omega \text{ cm}^2$ (EIS 4) to $4500 \Omega \text{ cm}^2$ (EIS 6) and a decreasing capacitance from $0.15 \times 10^{-7} \text{ F cm}^2$ (EIS 4) to $0.06 \times 10^{-7} \text{ F cm}^2$ (EIS 6) of the barrier oxide layer could be interpreted as an ongoing film growth. This is, however, not observed in TEM investigations. Naively applying Eq. (4) to the EIS data and assuming a relative dielectric number of $\epsilon_r = 9$ would result in an unreasonably large thickness of the barrier layer: 191 nm at EIS 6. This clearly differs from the TEM measurements of 31.3 nm (Table 5b).

However, the results from EIS can be brought into good agreement with the observations by cryo-SEM if the formation of a blocking layer above the anodic oxide is taken into account. This leads

to a reduction of the active area of tape anodization. A determination of the degree of coverage θ is possible by comparing barrier layer resistance and capacitance of tape anodization with the corresponding values of bath anodization. The calculation of θ according to Eq. (6) and (7) is based on the assumptions that the oxide barrier layers of bath and tape anodization are nearly similar under the same conditions and that no partial blocking of the active area occurs for bath anodization.

$$\theta_C(EISx) = 1 - \frac{C_{tape,EISx}}{C_{bath,EISx}} \tag{6}$$

$$\theta_R(EISx) = 1 - \frac{R_{bath,EISx}}{R_{tape,EISx}} \tag{7}$$

The degree of coverage θ during the different stages of anodization is plotted in Figure 9. The results for two different runs with anodization tape are shown. The capacitance and resistance for bath anodization were determined as the average of two bath anodization processes.

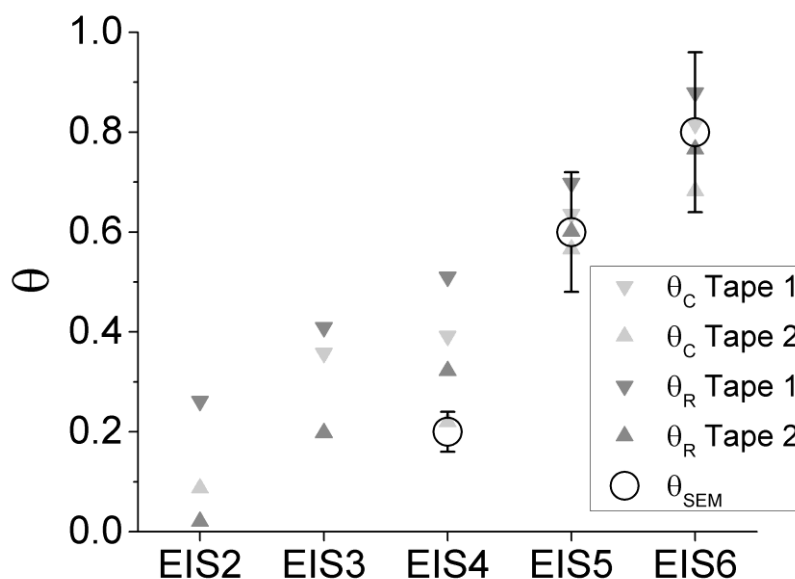


Figure 9. Degree of coverage during tape anodization calculated by Eq. 6 (θ_C) and Eq. 7 (θ_R) with an average error of smaller than 5% (not shown) and by visual estimation of cryo-SEM images (Figure 5) with an average error of 20%

For both tape anodization runs, the degree of coverage increases with increasing voltage between EIS 2 and EIS 4 and with increasing time for constant voltage between EIS 4 and EIS 6. At the beginning of the tape anodization (EIS 2, 3 V), the degree of coverage is still moderate with a value of about 25%. Finally, for EIS 6 (25 V, 20 min) about 80% of the anodic oxide surface is covered. These results fit well with the coverage data obtained by an image analysis of the cryo-SEM micrographs (Figure 5).

In their paper, Jüttner and Lorenz [12] proposed several theoretical models for the analysis of EIS data obtained on metals with an oxide surface. This surface is covered by an additional layer with punctual defects. The models were originally developed in the context of electrochemical corrosion, but as will be shown in the following they can also be applied to the situation of tape anodization.

The electrical equivalent circuit for one particular model is shown in Figure 10. It contains elements for describing both an anodic oxide layer (R_{barrier} , C_{barrier} , R_{pores}) as well as a layer that locally blocks the oxide (R_{blocking} , C_{blocking}). $R_{\text{pores,blocking}}$ relates to the electrical current flowing through the openings in the blocking layer. The degree of coverage is characterized by the parameter θ , which varies between 0 (no coverage of anodic oxide) and 1 (anodic oxide fully blocked).

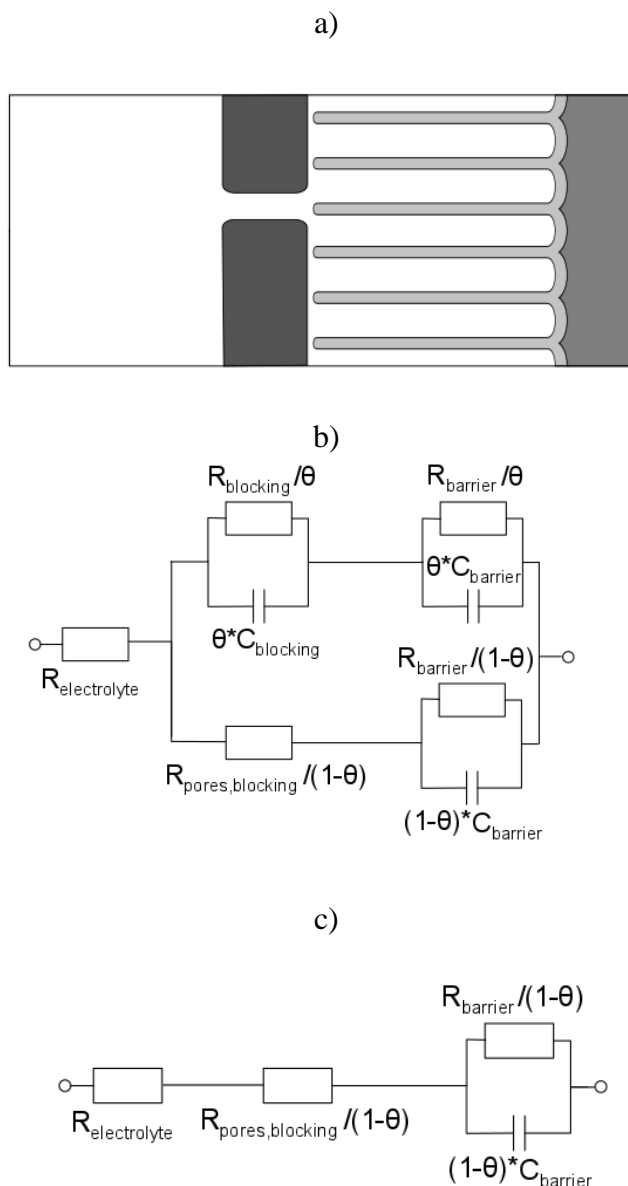


Figure 10. a) Schematic illustration of the “passive pit model” [12]; b) equivalent electrical circuit originally proposed by [12]; c) reduced equivalent electrical circuit assuming a thick blocking layer ($R_{\text{blocking}} \rightarrow \infty$ and $C_{\text{blocking}} \rightarrow 0$)

In this work we further simplified the model by assuming that the blocking layer has a much larger thickness than the underlying anodic oxide. For the cloud-like layer that forms during tape anodization, this assumption is clearly justified, as demonstrated by cryo-SEM (cf.). Here, R_{blocking} becomes very large and C_{blocking} very small, so that the upper branch of the original equivalent circuit

can be neglected, thus obtaining the reduced equivalent circuit shown in Figure 10c. According to this model, the resistance and capacitance of the barrier oxide can be directly measured under the condition of zero surface coverage.

As stated above, this condition is fulfilled when anodization is carried out in a bath, where no residues on the surface are produced. Hence, R_{bath} and C_{bath} in equations (6) and (7) can be identified as R_{barrier} and C_{barrier} . Using this and the equivalent circuit in Figure 10c we arrive at

$$R_{\text{tape}} = \frac{R_{\text{bath}}}{(1-\Theta)} C_{\text{tape}} = C_{\text{bath}} \cdot (1 - \Theta) \quad (8)$$

which is completely equivalent to equations (6) and (7). Therefore, the procedure we used for evaluating the degree of coverage from the EIS data is essentially conforming to a simplified version of the model introduced by Jüttner and Lorenz.

4. CONCLUSION

Anodization using a newly developed adhesive tape is a convenient method for the local surface treatment of aluminum before painting or adhesive bonding. The anodic oxide layers produced by the tape exhibit the same morphology as the anodic oxide layers from conventional anodization in a bath (phosphoric acid process). The thicknesses of the base oxide and the porous oxide for different voltages and anodization times are also comparable.

In this work, we carried out a more detailed investigation of the tape anodization process by employing cryo-SEM and *in-situ* EIS. Cryo-SEM shows the formation of a cloud-like layer partly covering the anodic oxide. Since the degree of coverage increases with anodization time, the cloud-like layer probably consists of reaction products from the anodization process. It could be expected that the residues contain high concentrations of aluminum phosphate, which has a low solubility, but EDX measurements indicate that the amount of aluminum in the residues is not particularly high. The exact chemical nature of the residues is not known yet, but EDX data are compatible with the assumption that it consists of an organic gel which is possibly stabilized by aluminum ions.

In-situ EIS allows an on-line monitoring of the growth of the anodic oxide layer and, in the case of tape anodization, also gives information about the build-up to the cloud-like surface layer. Data for the capacitance of the barrier layer C_{barrier} and its resistance R_{barrier} could be extracted from the high frequency part of the EIS spectra. For bath anodization, both values showed the expected increase with increasing anodization voltage, which reflects the thickening of the barrier oxide. When the dielectric permittivity number ϵ of the oxide is calculated from C_{barrier} and the thickness of the barrier oxide as it was obtained the TEM measurement, a good agreement with the data in the literature is found.

In the early stages of tape anodization, the EIS data for the tape closely resemble the data obtained in the bath. Later on (at the beginning of the 25 V plateau) deviations become apparent, which steadily increase with time. Namely, C_{barrier} and R_{barrier} take values that would correspond to a barrier layer with unrealistically high barrier thickness or permittivity number. These results can be understood by applying a model proposed by Jüttner and Lorenz [12], which accounts for a partial blocking of the anodic oxide by an additional surface layer. The degree of coverage obtained by

analyzing the EIS data in terms of the Jüttner model closely agrees with the percentage of the surface covered by the cloud-like layer, which was estimated on the basis of cryo SEM micrographs.

Therefore, it turns out that *in-situ* EIS is a valuable tool to study the accumulation of reaction products on an aluminum surface during the anodization process. The effect is especially pronounced in the case of tape anodization because here all mass transport processes are limited by the extremely high viscosity of the electrolyte of the tape adhesive.

ACKNOWLEDGEMENTS

The authors would like to thank Antonina Krieger for her preparation of the anodization tapes.

References

1. J.C. Norris, *Plat. and Surf. Finishing*, 78 (1991) 36.
2. J.C. Norris, *Galvano organo traitements de surface*, 64 (1995) 141.
3. C.L. Ong, W.Y. Shu and S.B. Shen, *Int. J. Adhes. Adhes.* 12 (1992) 79.
4. http://www.dalicworld.com/dalicstick_gb.html
5. L. Bergan, *Int. J. Adhes. Adhes.* 19 (1999) 199.
6. M. Burchardt, S. Dieckhoff, A. Hartwig, M. Kleemeier, K. Teczyk, P. Vulliet and A. Fangmeier, European Patent EP2689052B1 (2016).
7. L. Berndt, A. Hartwig, M. Kleemeier, A. Krieger, K. Thiel and M. Burchardt, *Surf. Interface Anal.* 48 (2016) 926.
8. R. Wilken, S. Dieckhoff, A. Hartwig and M. Kleemeier, European Patent EP1913180B1 (2011).
9. M. Itagaki, N. Kobari, S. Yotsuda, K. Watanabe and S. Kinoshita, *J. Power Sources* 135 (2004) 255.
10. A. Amirudin and D. Thierry, *Prog. Org. Coat.*, 26 (1995) 1.
11. F. Mansfeld, *J. Appl. Electrochem.* 25 (1995) 187.
12. K. Jüttner and W.J. Lorenz, *Mater. Sci. Forum* 44-45 (1990) 191.
13. B.-Y. Chang and S.-M. Park, *Annu. Rev. Anal. Chem.* 3 (2010) 207.
14. S.-M. Park and J.-S. Yoo, *Anal. Chem.* 75 (2003) 455 A.
15. A. Mazzarolo, M. Curioni, A. Vincenzo, P. Skeldon and G.E. Thompson, *Electrochim. Acta* 75 (2012) 288.
16. M. Curioni, E.V. Koroleva, P. Skeldon and G.E. Thompson, *Electrochim. Acta* 55 (2010) 7044.
17. L. Hua, J. Liu and S. Li, *Int. J. Electrochem. Sci.*, 10 (2015) 2194.
18. B.H. Linden, H. Terryn, and J. Vereecken, *J. Appl. Electrochem.* 20 (1990) 798.
19. P.G. Sheasby, R. Pinner, and S. Wernick, *The surface treatment and finishing of aluminium and its alloys*, ASM International, (2001) UK.
20. M. v. Put, *Potentiodynamic anodizing and adhesive bonding of aluminium for the aerospace industry*, in *Department of Materials Science and Engineering*, Delft University of Technology (2013) Delft.
21. W. Lee, K. Schwirn, M. Steinhart, E. Pippel, R. Scholz and U. Gosele, *Nat. Nanotechnol* 3 (2008) 234.
22. W. Lee, R. Ji, U. Gosele and K. Nielsch, *Nat. Mater.* 5 (2006) 741.
23. J.W. Diggle, T.C. Downie and C. Goulding, *Chem. Rev.* 69 (1969) 365.
24. J.P. O'Sullivan and G.C. Wood, *Proc. R. Soc. London, Ser. A*, 317 (1970) 511.
25. A. Amore Bonapasta, F. Buda and P. Colombet, *Chem. Mater.* 12 (2000) 738.
26. X. Zhu, Q. Gao, D. Xu and X. Shi, *J. Appl. Polym. Sci.* 113 (2009) 143.
27. E. Ringenbach, G. Chauveteau, and E. Pefferkorn, *J. Colloid Interface Sci.* 161 (1993) 223.

28. L.R.B. Holzle, D.S. Azambuja, C.M.S. Piatnicki and G.E. Englert, *Mater. Chem. Phys.* 103 (2007) 59.
29. M. Metikoš-Huković, R. Babić, and Z. Grubač, *J. Appl. Electrochem.* 32 (2002) 35.
30. I.V. Aoki, M.C. Bernard, S.I.C. de Torresi, C. Deslouis, H.G. de Melo, S. Joiret and B. Tribollet, *Electrochim. Acta* 46 (2001) 1871.
31. A.G. Muñoz and J.B. Bessone, *Corros. Sci.* 41 (1999) 1447.
32. H.J.W. Lenderink, M.V.D. Linden and J.H.W. De Wit, *Electrochim. Acta* 38 (1993) 1989.
33. J.B. Bessone, D.R. Salinas, C.E. Mayer, M. Ebert and W.J. Lorenz, *Electrochim. Acta* 37 (1992) 2283.
34. C.M.A. Brett, *J. Appl. Electrochem.* 20 (1990) 1000.
35. S.E. Frers, M.M. Stefenel, C. Mayer and T. Chierchie, *J. Appl. Electrochem.* 20 (1990) 996.
36. J. Bessone, C. Mayer, K. Juttner and W.J. Lorenz, *Electrochim. Acta* 28 (1983) 171.
37. B. Cheng, S. Ramamurthy, and N.S. McIntyre, *J. Mater. Eng. Perform.* 6 (1997) 405.
38. J.W. Schultze, M.M. Lohrengel, and D. Ross, *Electrochim. Acta* 28 (1983) 973.
39. C.M.A. Brett, I.A.R. Gomes and J.P.S. Martins, *J. Appl. Electrochem.* 24 (1994) 1158.
40. E.J. Lee and S.I. Pyun, *Corr. Sci.* 37 (1995) 157.
41. I. Epelboin and M. Keddam, *J. Electrochem. Soc.* 117 (1970) 1052.
42. H.-J. Oh, K.-W. Jang and C.-S. Chi, *Bull. Korean Chem. Soc.* 20 (1999) 1340.
43. A. Girginov, A. Popova, I. Kanazirski, A. Zahariev, *Thin Solid Films* 515 (2006) 1548.
44. J. P. Dasquet, D. Caillard, J. P. Bonino, R.S. Bes, *J. Mater. Sci.* 36 (2001) 3549.
45. A.J. Bard, M. Stratmann and G. Frankel, *Encyclopedia of Electrochemistry. Volume 4: Corrosion and Oxide Films*, Wiley-VCH,(2003) Weinheim.

© 2018 The Authors. Published by ESG (www.electrochemsci.org). This article is an open access article distributed under the terms and conditions of the Creative Commons Attribution license (<http://creativecommons.org/licenses/by/4.0/>).